UvA-DARE (Digital Academic Repository)

Non-invasive determination of port wine stain anatomy and physiology for optimal laser treatment strategies

van Gemert, M.J.C.; Nelson, J.S.; Milner, T.E.; Smithies, D.J.; Verkruijsse, W.; de. Boer, J.F.; Lucassen, G.W.; Goodman, D.M.; Tanenbaum, B.S.; Norvang, L.T.; Svaasand, L.O.

[Link to publication](#)

Non-invasive determination of port wine stain anatomy and physiology for optimal laser treatment strategies

Martin J C van Gemert†‡, J Stuart Nelson†+, Thomas E Milner†,
Derek J Smithies†, Wim Verkruysse‡, Johannes F de Boer‡,
Gerald W Lucassen‡, Dennis M Goodman§, B Samuel Tanenbaum†‖,
Lill T Norvang¶ and Lars O Svaasand¶

† Beckman Laser Institute and Medical Clinic, Irvine, CA, USA
‡ Laser Centre, Academic Medical Centre, Amsterdam, The Netherlands
§ Lawrence Livermore National Laboratory, Livermore, CA, USA
‖ Harvey Mudd College of Engineering, Claremont, CA, USA
¶ Division of Physical Electronics, University of Trondheim, Norwegian Institute of Technology,
Trondheim, Norway

Abstract. The treatment of port wine stains (PWSs) using a flashlamp-pumped pulsed dye laser is often performed using virtually identical irradiation parameters. Although encouraging clinical results have been reported, we propose that lasers will only reach their full potential provided treatment parameters match individual PWS anatomy and physiology. The purpose of this paper is to review the progress made on the technical development and clinical implementation of (i) infrared tomography (IRT), optical reflectance spectroscopy (ORS) and optical low-coherence reflectometry (OLCR) to obtain *in vivo* diagnostic data on individual PWS anatomy and physiology and (ii) models of light and heat propagation, predicting irreversible vascular injury in human skin, to select optimal laser wavelength, pulse duration, spot size and radiant exposure for complete PWS blanching in the fewest possible treatment sessions. Although non-invasive optical sensing techniques may provide significant diagnostic data, development of a realistic model will require a better understanding of relevant mechanisms for irreversible vascular injury.

1. Introduction

Port wine stains (PWSs) are congenital, vascular malformations of the dermis, that occur in an estimated five children per 1000 births (Mulliken and Young 1988). PWSs should not be considered a cosmetic problem *per se* but a disease with potentially devastating psychological and physical complications. Personality development is adversely influenced in virtually all patients by the negative reaction of others to a 'marked' person (Tan 1992).

Using appropriate light dosimetry, flashlamp-pumped pulsed dye lasers can selectively destroy cutaneous blood vessels. Although results of clinical studies are encouraging (see e.g. Tan 1992), recent experience shows that only a small proportion of patients (10–20%) obtain 100% fading of their PWS, even after undergoing multiple treatments. We propose that the primary reason for inadequate clinical results is that all PWSs are treated with virtually identical laser parameters, which may not be appropriate on an individual patient

+ Correspondence: J Stuart Nelson, Beckman Laser Institute and Medical Clinic, 1002 Health Sciences Road East, Irvine, CA 92715, USA. E-mail address: snelson@bli.uci.edu

basis. Now that laser systems are available that allow user-specified selection of irradiation parameters, non-invasive optical and thermal sensing techniques must be developed that document the anatomical and physiological characteristics of the PWS. From these data, using realistic models of light and heat transport which predict irreversible vascular injury in PWS skin, optimal irradiation parameters can be selected on an individual patient basis throughout an extended treatment protocol.

The purpose of this paper is twofold: first, to review the progress on technical development and clinical implementation of three non-invasive sensing methods to obtain *in vivo* data on the biophysical, structural, optical and thermal properties of human PWS skin; second, to review the progress on optical–thermal models which predict irreversible damage of PWS blood vessels in response to pulsed laser exposure. These computations must provide the information necessary to select the optimal wavelength (λ_0 (nm)), pulse duration (t_L), and radiant exposure (J cm^{-2}) for complete PWS blanching in the fewest possible treatment sessions.

2. Port wine stains

Histopathological studies of PWSs show a normal epidermis overlying an abnormal plexus of dilated dermal blood vessels. Epidermal melanin concentration, distribution of vessel number and diameter as a function of depth, percentage oxygen saturation and blood flow velocity are important anatomical and physiological characteristics, that vary on a site to site and individual patient basis, on the same PWS.

The predominant endogenous skin chromophores absorbing light at the clinically relevant wavelengths are melanin and blood. Melanin absorption is strongest in the ultraviolet, decreasing rapidly through the visible and near-infrared approximately as $1/\lambda^4$ (Svaasand *et al* 1995b). The coefficient of blood absorption, $\mu_{a,bl}$ (mm^{-1}), which is dependent on wavelength and percentage oxygen saturation, is significantly greater than the coefficient of scattering for $\lambda < 600$ nm (Svaasand *et al* 1995b). Consequently, the optical penetration depth for such wavelengths in blood is approximately equal to $1/\mu_{a,bl}$. Furthermore, in the green–yellow spectral region (500–600 nm) the penetration depth in whole blood (41% haematocrit) is 30–50 μm, which corresponds to the diameter of moderate-sized PWS vessels. Therefore, light propagation in PWS skin depends on the fractional blood volume and vessel diameter (Svaasand *et al* 1995a, Verkruysse *et al* 1997).

3. Non-invasive methods to determine PWS anatomy and physiology

Optimization of PWS laser treatment on an individual patient basis requires development of diagnostic methods to determine epidermal melanin concentration, distribution of vessel number and diameter as a function of depth, percentage oxygen saturation and blood flow velocity. Although alternative diagnostic sensing techniques are under development (e.g., high frequency ultrasound and photoacoustic imaging), three non-invasive diagnostic sensing methods that provide important optical–thermal data to determine PWS anatomy and physiology, and which are amenable to laboratory testing and clinical implementation, are reviewed. These are infrared tomography (IRT), subsection 3.1; optical reflectance spectroscopy (ORS), subsection 3.2, and optical low-coherence reflectometry (OLCR), subsection 3.3.

3.1. Infrared tomography (IRT)

IRT uses a fast infrared focal plane array (IR FPA) camera to detect the increase in infrared emission at the tissue surface, which is induced by instantaneous heating of subsurface chromophores and susbsequent thermal diffusion. The chromophores' lateral physical dimensions are best resolved from the early frames in the time sequence of infrared emission images when thermal diffusion is limited.

The IRT integral equation (1) below can be written as a multi-dimensional convolution integral that relates the measured time sequence of infrared emission images, $\Delta M(x, y; t)$ (°C), where $x, y; t$ are the tissue surface coordinates and time, respectively, to the initial space-dependent temperature increase, $\Delta T_{chr}(\xi, \eta, \zeta; t = 0)$ (°C), of the subsurface chromophores at position (ξ, η, ζ), immediately following pulsed laser exposure (pulse ends at $t = 0$). Here, the ξ, η and x, y axes are coincident and $\zeta = 0$ coincides with the tissue surface. So, we can write

$$\Delta M(x, y; t) = \int_{x'} \int_{y'} K_c(x - x', y - y') \, dx' \, dy' \int_\xi \int_\eta \int_\zeta K_T(x' - \xi, y' - \eta, \zeta; t)$$
$$\times \Delta T_{chr}(\xi, \eta, \zeta; t = 0) \, d\xi \, d\eta \, d\zeta. \tag{1a}$$

Formally, this equation can be written as a product of two convolution operations, one (K_c) acting over the surface, and the other (K_T) inside the tissue,

$$\Delta M = K_c * K_T * \Delta T_{chr} \tag{1b}$$

where $K_c(x - x', y - y')$ (m^{-2}) and $K_T(x - \xi, y - \eta, \zeta; t)$ (m^{-3}) represent, respectively, the camera and thermal point spread (i.e., Green's) functions. Analysis of $\Delta M(x, y; t)$ by longitudinal inversion and lateral deconvolution algorithms (Milner *et al* 1995, 1996a, b) provides a direct means to determine the depths and lateral physical dimensions of subsurface chromophores.

The camera point spread function (K_c) describes the inherent limitations of the IR FPA camera which includes effects due to size of the collection aperture, lens aberrations, finite number and size of discrete detector elements (Hopper 1993).

Assuming a Dirac delta thermal source of unit strength embedded in a biological material at coordinates (ξ, η, ζ), solution of the bio-heat equation gives the thermal point spread function K_T,

$$K_T(x - \xi, y - \eta, \zeta; t) = K_r(x - \xi, y - \eta; t) K_z(\zeta; t) \tag{2}$$

where K_T is the product of the two terms (3a) and (3b) below, representing, respectively, heat diffusion along lateral (K_r (m^{-2}) and longitudinal (K_z (m^{-1})) axes (Milner *et al* 1996a)

$$K_r(x - \xi, y - \eta; t) = \frac{1}{\pi(2\sigma_s^2 + 4\chi t)} \exp[-((x - \xi)^2 + (y - \eta)^2)/(2\sigma_s^2 + 4\chi t)] \tag{3a}$$

$$K_z(t; \zeta) = \frac{\mu_{ir} \exp(-\zeta^2/4\chi t)}{2} \left\{ \text{erfcx}(u_+) + \text{erfcx}(u_-) \right.$$
$$\left. - \frac{2(h/\kappa)}{(h/\kappa) - \mu_{ir}} [\text{erfcx}(u_+) - \text{erfcx}(u_1)] \right\} \tag{3b}$$

where

$$u_\pm = \mu_{ir}\sqrt{\chi t} \pm \zeta/2\sqrt{\chi t} \qquad u_1 = (h/\kappa)\sqrt{\chi t} \pm \zeta/2\sqrt{\chi t} \tag{3c}$$

σ_s, χ, h and κ represent, respectively, infrared scattering length (m^{-1}), thermal diffusivity (m^2 s^{-1}), heat loss coefficient (W m^{-2} K^{-1}) and thermal conductivity of human

skin (W m^{-1} K^{-1}). Furthermore, erfcx$(u) = \exp(u^2)$ erfc(u), where erfc(u) is the complementary error function [1-erf(u)].

The IRT integral equation (1) represents a *forward* problem in which $\Delta M(x, y; t)$ may be computed from the initial space-dependent temperature increase, $\Delta T_{chr}(\xi, \eta, \zeta; t = 0)$, and the known biophysical properties of human skin. As the only available input data are a time sequence of measured infrared emission images ($\Delta M(x, y; t)$), $\Delta T_{chr}(\xi, \eta, \zeta; t = 0)$ is determined from

$$\Delta T_{chr} = (K_z)^{-1}(K_c * K_r)^{-1}\Delta M \tag{4}$$

which constitutes the *inverse* problem of the IRT integral equation (1).

Computationally efficient *one-dimensional* longitudinal inversion and *two-dimensional* lateral deconvolution algorithms have been developed. The initial temperature increase is always positive (i.e., $\Delta T_{chr} \geqslant 0$), so a *non-negative constrained conjugate gradient algorithm* is used for improved solution estimates (Goodman *et al* 1992).

Use of a high-speed IR FPA camera system to image individual laser-heated blood vessels has been demonstrated and the performance of longitudinal inversion and lateral deconvolution algorithms tested in preliminary studies in PWS patients. A compound infrared lens ($f/5$, 50 mm diameter) imaged the surface increase in infrared emission intensity from PWS skin onto a 128×128 InSb IR FPA. Immediately following pulsed exposure (wavelength, 585 nm; pulse duration $t_L = 0.45$ ms; spot size, 5 mm; radiant exposure, 5.0 J cm^{-2}), the IR FPA camera system recorded a timed sequence of 126 infrared emission images $\Delta M(x, y; t)$. From this sequence, the *one-dimensional* quantity $\Delta M^{1-D}(t)$ was determined (figure 1(A)) by averaging over an area ($\delta A = 1.5$ mm^2) positioned at the centre of laser exposure. Using the algorithm, the longitudinal inverse problem was solved (figure 1(B)) for the initial *one-dimensional* temperature increases, $\Delta T_{chr}^{1-D}(z; t = 0)$, in the epidermal melanin layer and deeper PWS blood vessels. Depths of the epidermal melanin layer ($50 \pm 25 \ \mu$m) and deeper PWS blood vessels ($275 \pm 75 \ \mu$m) (figure 1(B)) match the mean depths measured from histopathologic analysis (Milner *et al* 1996b).
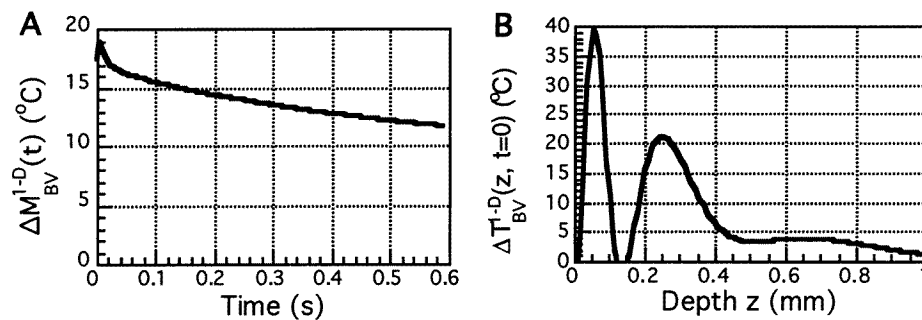
Figure 1. (A) Measured IR emission, $\Delta M^{1-D}(t)$. (B) Depths of the epidermal melanin layer ($50 \pm 25 \ \mu$m) and PWS blood vessels ($275 \pm 75 \ \mu$m) determined by the longitudinal inversion algorithm match the mean depths measured directly using histopathology (Milner *et al* 1996b).

For the same PWS site, $\Delta M(x, y; t_0 = 77$ ms) was measured (figure 2(A)). IR emission exclusively from the deeper discrete PWS blood vessels is computed (figure 2(B)) by subtracting from $\Delta M(x, y; t_0 = 77$ ms) the infrared emission due to epidermal melanin heating. Solution of the lateral deconvolution problem (ΔT_{chr}^{2-D}) using the subtracted image as input data allows determination of the lateral physical dimensions, 150–200 μm, of

the deeper discrete laser-heated PWS blood vessels (figure 2(C)). The mean temperature increase, $\langle \Delta T \rangle = 48\,°C$, of these vessels was computed from the fractional blood vessel area, $f = 0.42$, in the deconvolved infrared emission image and *one-dimensional* temperature increase $\Delta T_{chr}^{1-D}(z; t = 0)$ as determined from, respectively, the solutions of the lateral deconvolution and longitudinal inversion algorithms.
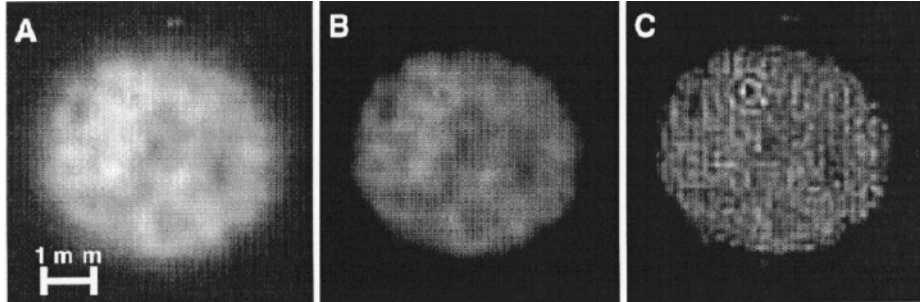
Figure 2. (A) Measured IR emission image $\Delta M(x, y; t_0 = 77\ \text{ms})$. (B) IR emission exclusively from the deeper discrete PWS blood vessels computed after application of the layer-stripping method. (C) Solution of the lateral deconvolution problem ΔT_{chr}^{2-D} using image (B) as input data; lateral physical dimensions of the discrete PWS blood vessels were determined by the lateral deconvolution algorithm to be 150–200 μm.

The rationale for using IRT in the clinical management of patients is that the technique offers a direct means of documenting the PWS vascular characteristics on a site to site basis for each patient. We propose that, prior to the institution of therapy, analysis of $\Delta M(x, y; t)$ in response to a sub-therapeutic diagnostic laser pulse, provides information on (i) the initial space-dependent temperature increase $\Delta T_{chr}(\xi, \eta, \zeta; t = 0)$ within the blood vessels immediately following pulsed laser exposure and (ii) depths and physical dimensions of the most superficial absorbing PWS blood vessels. Such information can then be used by the clinician to help select the optimal parameters (wavelength, pulse duration and radiant exposure) for the first laser treatment. At the next treatment session, a second IRT record is made. Because many of the most superficial vessels were removed by the first laser treatment, IRT now images a deeper absorbing layer of PWS blood vessels. The optimal parameters (wavelength, pulse duration and radiant exposure) for the second laser exposure are selected based on analysis of the IRT record and a second treatment performed. Proceeding in this manner, the IRT record probes deeper absorbing layers of the PWS after the most superficial blood vessels are removed by each successive treatment at the same site.

3.2. Optical reflectance spectroscopy (ORS)

ORS uses diffuse white-light irradiation to detect the backscattered (reflected) light from the PWS skin at visible and near-infrared wavelengths. The reflection spectrum contains information regarding visual appearance of the lesion and is dependent on the skin optical and anatomical properties including epidermal and dermal scattering coefficients, the quantities of epidermal melanin and other chromophores and, in particular, the distribution of vessel number and diameters of normal and PWS blood vessels as a function of depth. The long-term objective is to develop ORS for clinical use. This requires solution of the ORS *inverse* problem to determine skin optical and anatomical characteristics.

Before attempting to solve the inverse problem, calculation of reflectance spectra using various simulated sets of vascular anatomies and optical absorption and scattering properties is necessary (the *forward* problem). This requires calculation of the fluence rate distribution in model PWS skin between 400 and 700 nm wavelengths where the magnitude of the blood absorption coefficient changes by a factor of over 1000. Two approaches have been successfully used to predict realistic reflectance spectra. The first applies optical diffusion theory to model light propagation in PWS skin with dermal layers of different homogeneous blood concentrations (Svaasand *et al* 1995b). Measured and simulated reflectance spectra (figure 3(A)) of normal skin and untreated and treated PWSs (Norvang *et al* 1996) show characteristic differences. From such data, Svaasand *et al* (1995b) concluded that as vessel depth increases the PWS darkens progressively from bright red (< 0.4 mm), to deep red (0.4–0.5 mm), and finally to bluish-purple (> 0.5 mm). The second approach applies efficient Monte Carlo computations of the fluence rate distribution in model PWS skin, containing numerous vessels (Verkruysse *et al* 1997). Figure 3(B) shows the calculated fluence rate distributions at 577 and 585 nm wavelengths for a 10% dermal fractional blood volume and figure 3(C) depicts computed ORS using several vessel diameters (Verkruysse *et al* 1996 unpublished).

The ORS *inverse* problem has not (yet) been solved and part of our effort is to infer what detailed anatomical data can be derived given the PWS reflectance spectrum. Preliminary work on the wavelength dependence of ORS suggests that $\lambda > 700$ nm gives information on the dermal fractional blood volume, whereas $500 < \lambda < 600$ nm and $\lambda < 500$ nm specify the average diameter of deeper and superficial PWS vessels, respectively. In addition, the absorption coefficient of epidermal melanin may be inferred from ORS. Finally, ORS can be used to determine quantitatively the degree of PWS blanching following each laser treatment.

### 3.3. Optical low-coherence reflectometry (OLCR)

OLCR is a technique (Huang *et al* 1991) whereby the location and relative strength of optically scattering structures can be deduced. Results from OLCR are analogous to those from an ultrasound B-scan except that the imaging is performed optically instead of acoustically. However, OLCR is far superior to ultrasound for imaging thin, superficial structures in that the techniques is non-contact, has high sensitivity (signal to noise ratios (SNR) > 100 dB) and, most importantly, high spatial resolution of 1–10 μm in both the axial and radial directions.

In practice, light emitted form a low-coherence source is coupled into a two-beam fibre optic interferometer and split into sample and reference paths. Light backscattered by the test material recombines with that retroreflected from the reference to produce constructive interference only for coherent photons that have a time-of-flight difference which matches the reference-target optical delay to within the source coherence length (Goodman 1985).

Within the last decade, there has been a considerable increase in the application of non-invasive optical techniques such as laser Doppler flowmetry (LDF) to study skin microcirculation (see, e.g., Bonner and Nossal 1990). Unfortunately, LDF provides only global information on dermal blood flow and does not reveal specific data relevant to discrete spatial locations in skin.

If we assume that the measured OLCR signal, $I(z; t)$, at reference mirror position z, is exclusively due to singly scattered photons, then we find

$$I(z; t) = 2A_0 \int_0^\infty |\gamma_{0,bs}(\tau_f)| \cos[2\pi(\nu_m + \nu_d(z))t] d(\overline{\varepsilon_0 A_{bs}})(z'). \qquad (5)$$
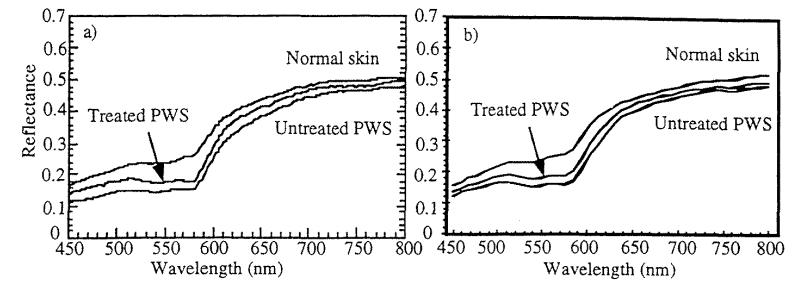
(A)
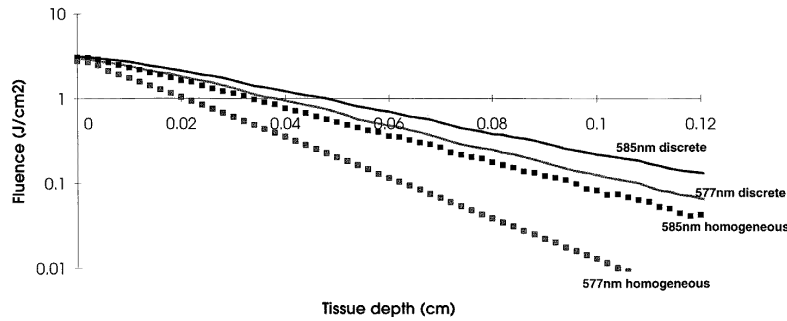
(B)
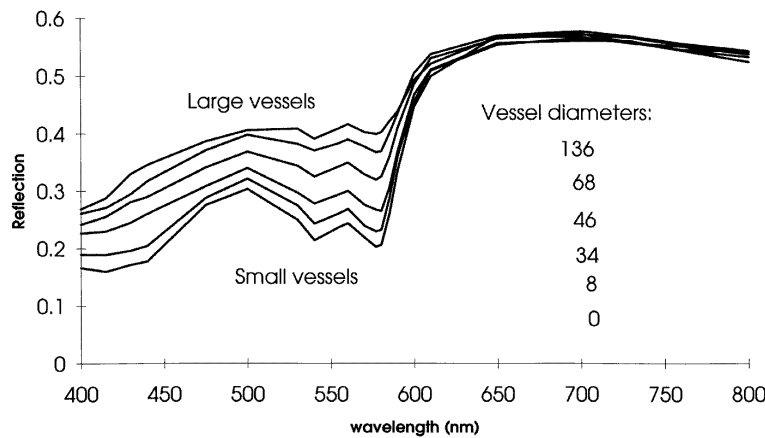

(C)

Figure 3. (A) (a) Measured and (b) simulated reflectance spectra of a reddish-purple PWS (Norvang *et al* 1996). Treatment was carried out 6 weeks before the measurement of the 'treated PWS'. (B) Computed fluences at 577 and 585 nm wavelengths in two PWS models with a 60 μm thick epidermis. The first consists of discrete 36 μm diameter blood vessels located in adjacent columns at dermal depths of 100, 300, 500, 700 μm, etc, and 200, 400, 600 μm etc, from the epidermal–dermal junction, and 10% partial dermal fractional blood volume. The second consists of a 10% continuous partial dermal fractional blood volume. Epidermal absorption and scattering were 0.6 mm^{-1} and 50 mm^{-1}, $g = 0.8$, respectively; dermal parameters were 0.03 mm^{-1}, 25 mm^{-1} and 0.8, respectively. (C) Computed reflectance spectra in a 60 μm epidermis model PWS model, and a 380 μm dermal layer with 5% partial blood volume in vessel diameters varying between 136, 68, 46, 34, 27.2, 8 and 0 μm. Below this dermal layer is another layer of 1.5 mm with 1% partial dermal fractional blood volume.

Here, A_0 is the source amplitude retroreflected from the reference arm; $\gamma_{0,bs}(\tau_f)$ is the complex degree-of-coherence function between the source and Doppler broadened backscattered light with a time-of-flight difference, $\tau_f = 2(z - z')/c$, where z and z' are the optical pathlengths in the reference and probe arms, respectively; ν_m and $\nu_d(z')$ are, respectively, the frequency of the phase modulation and moving red blood cells at position z'; $d(\overline{\varepsilon_0} \overline{A_{bs}})(z')$ is the differential backscattered light amplitude from a region of thickness dz' in the test material at position z' and collected by the target fibre probe; $\overline{\varepsilon_0}$ is the Jones vector representing the polarization state of light retroreflected from the reference; $\overline{A_{bs}}$ is the backscattered light amplitude vector. Effects of Doppler shift, scattering and absorption on the OLCR signal are contained in equation (5). Due to transmission losses (scattering and absorption), $|A_{bs}|$ generally decreases exponentially with increasing skin depth but also rises and falls in proportion to local variations in the refractive index. Because features 1–2 mm deep in skin may be imaged using OLCR, frequency and amplitude changes of backscattered light from blood can be easily identified. When light is backscattered from a vessel containing moving red blood cells (RBCs), $|\nu_d(z')|$ increases, which shifts and broadens the OLCR signal frequency about ν_m. Raster scanning light from the target fibre probe allows construction of a three-dimensional tomographic map of the underlying skin microcirculation. In contrast to LDF, the overall OLCR signal due to moving RBCs is almost entirely due to the Doppler shifted and broadened backscattered light. As a result, signal-to-noise ratio (SNR) is expected to be substantially higher than LDF.

To investigate the application of OLCR for measuring fluid flow embedded in scattering media, velocity profiles within a turbid cylindrical collagen conduit have been measured. Light in the target arm is focused into a test conduit carrying a flowing fluid that contains polymer microspheres suspended in water forced through the collagen conduit by a linear syringe pump. The collagen wall represents an optical scattering barrier similar to that found in human skin. Circular symmetry results in the development of a parabolic velocity flow profile in the cylindrical conduit. Velocity profiles corresponding to two pump speeds were measured across a central diameter of the collagen conduit. Theoretical fits to a parabolic function for both velocity profiles are in excellent agreement with measured values (figure 4). Additionally, the inner diameter ($d = 940$ μm) and wall thickness (210 μm) of the cylindrical collagen conduit may be determined from the OLCR scan.

Although OLCR would allow real-time diagnostics, scan times are limited by the Doppler shift of backscattered light from moving RBCs. For example, for $\nu_d = 1$ kHz, a 1 ms measurement time is required at each skin site. This permits a semi-quantitative evaluation of the efficiency of PWS laser therapy as a function of incident light dosage. If partial replenishment of flow occurs immediately or shortly after laser exposure, indicative of reperfusion due to inadequate blood vessel injury, the PWS can be retreated. This process is continued until the measured Doppler shift is zero due to a permanent reduction in blood flow after laser exposure, indicative of irreversible microthrombus formation.

4. Optimal treatment of PWSs with known vascular anatomy and physiology

In this section we review the progress on development of theoretical models of light and heat propagation in skin to select the optimal laser wavelength (λ_0), pulse duration (t_L), radiant exposure (J cm^{-2}), spot size and repetition rate (s^{-1}) for irreversible vascular injury, assuming the PWS anatomy is known.
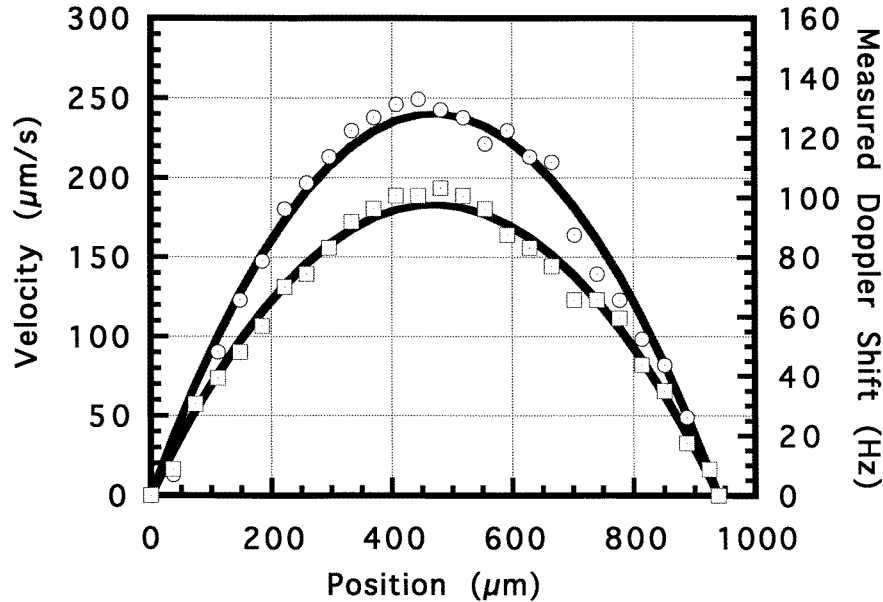
Figure 4. Experimental (circles and squares, two experiments) and theoretical parabolic (solid lines) velocity profiles in a turbid collagen conduit measured by OLCR.

4.1. Optimal wavelength (λ_0)

For individual treatment, λ_0 (nm) is defined so as to maximize the depth where targeted PWS blood vessels are irreversibly damaged by one laser pulse, leaving the epidermal–dermal junction (basal membrane) undamaged. As epidermal melanin absorption decreases with increasing wavelength, $\lambda_0 > 577$ nm is assumed. This can be formulated as (van Gemert *et al* 1995a, p 794)

$$\mu_{a,e}\phi(z_{e,d}) = \mu_{a,bl}(\lambda)\langle\phi(z_{bl})\rangle \qquad z_{bl} \text{ maximal for } \lambda = \lambda_0 > 577 \text{ nm} \quad (6)$$

where $\mu_{a,e}$ and $\mu_{a,bl}$ (mm^{-1}) are the absorption coefficients of epidermal melanin and blood respectively, ϕ (W mm^{-2}) denotes fluence rate, $z_{e,d}$ denotes the basal membrane depth, z_{bl} the top of the deepest blood vessel ($z = 0$ is the air–skin interface) and $\langle\phi(z_{bl})\rangle$ represents the average fluence rate distribution that results in irreversible damage to the deepest blood vessel at depth z_{bl}. Unfortunately, the mechanisms for irreversible blood vessel damage are, as yet, incompletely understood; this remains the most significant challenge for model development.

Equation (6) has been formulated (van Gemert *et al* 1995a, p 811), assuming that all blood is homogeneously distributed over the dermis. However, recent work (Svaasand *et al* 1995a, Verkruysse *et al* 1997) has shown that the homogeneous distribution assumption overestimates absorption by blood because red blood cells at the centre of the vessel absorb less light than those at the wall. Consequently, the vessel diameter, at constant dermal fractional blood volume, has a significant effect on $\langle\phi\rangle$.

This effect has been accounted for by reducing the homogeneously distributed dermal fractional blood volume by a correction factor (C), equal to the average fluence rate over the blood vessel cross section divided by the incident fluence rate (Verkruysse *et al* 1997). The result is that fluence rate distributions calculated in skin models with the corrected

dermal fractional blood volume are virtually identical to those with discrete blood vessels. An approximate expression for C (within $\pm 5\%$) is

$$C \approx \exp[-0.803(R\mu_{a,bl})] \qquad 0 \leqslant R\mu_{a,bl} \leqslant 1.5 \qquad (7a)$$

$$C \approx \exp[-0.983\sqrt{(R\mu_{a,bl})}] \qquad 1.5 < R\mu_{a,bl} \leqslant 4 \qquad (7b)$$

where R denotes vessel radius.

Assuming blood contained in the PWS vessels is homogeneously distributed over the dermis, previous analysis showed that the optimal wavelength for treatment (producing maximal heat at the top of a targeted vessel) shifts from 577 nm for lighter PWS to 585 nm and longer for darker lesions (van Gemert *et al* 1995b). If the correction factor (7) is included, however, heat production at the top of a targeted vessel is not significantly increased by shifting the wavelength from 577 to 585 nm. This prediction correlates with Monte Carlo computations of model PWS skin containing 50–100 μm diameter blood vessels (Smithies and Butler 1995, Lucassen *et al* 1996), predicting $\langle \phi(\lambda = 577 \text{ nm}) \rangle \approx \langle \phi(\lambda = 585 \text{ nm}) \rangle$.

Results of the current models are consistent with observations by Tan *et al* (1989) that at 585 nm deeper vascular injury is produced than at 577 nm in 1.8 mm thick pig skin (an estimated 2% dermal fractional blood volume contained in 10 μm diameter vessels; hence a correction factor C close to one, i.e. $C \approx 0.75$ at 577 nm and 0.86 at 585 nm). However, recent model predictions that 577 and 585 nm cause irreversible vessel damage at about the same skin depth in cases where the PWS consists of 50–100 μm diameter vessels are in contrast to reported clinical results (Tan *et al* 1990). This contradiction has, however, recently been solved by the authors (van Gemert *et al* 1997).

4.2. Optimal pulse duration (t_L)

Since the seminal papers by Anderson and Parrish (1981, 1983), the medical laser community has generally agreed that the optimal pulse duration causing irreversible damage to a blood vessel of radius R, but sparing the adjacent dermis, should match the vessel's thermal relaxation time τ (s), defined as

$$\tau = 4R^2/16\chi \qquad (8)$$

where χ is the thermal diffusivity of blood. This was recently verified in PWS patients by Dierickx *et al* (1995a). However, equation (8) is based upon the cooling behaviour of a model blood vessel in response to instantaneous heating of a line source located at the centre of the lumen. In this definition, τ is the time interval between the moment of instantaneous heating and occurrence of the peak temperature at the vessel wall (van Gemert *et al* 1995a, p 806).

Significant deviations from the prediction of Anderson and Parrish $\tau_L \approx \tau$ are obtained for the optimal pulse duration when the fluence rate distribution calculated by a Monte Carlo simulation is substituted in the heat conduction equation (neglecting acoustic effects which may become important for short pulse durations, i.e. close to 0.1 ms). The threshold radiant exposure necessary to raise the average temperature of a single vessel to 70 °C are plotted (figure 5) as a function of diameter ($2R$) for illumination times between 225 μs and 9.2 ms (Lucassen *et al* 1995, de Boer *et al* 1996). These curves show a distinct minimum in the threshold radiant exposure, which is least for the shortest illumination time, and ranges from 0.3 J cm^{-2} at 225 μs and $R = 15$ μm to 13 J cm^{-2} at 9.2 ms and $R = 40$ μm, at 577 nm. For 585 nm, where blood absorption is almost a factor of two smaller than at 577 nm, threshold radiant exposure is slightly higher, and occurs at slightly larger radii

(see de Boer *et al* 1996). As vessel diameter is decreased from this minimum, the thermal relaxation time becomes much shorter than the pulse duration (i.e. $\tau \ll t_L$). Here, a large fraction of the energy absorbed in the vessel is conducted to the surrounding tissue as heat. Consequently, the requisite fluence for irreversible vascular injury increases as the vessel diameter decreases. When the diameter increases from the minimum with constant pulse duration, the blood volume to be heated increases, so a higher fluence is required to achieve an average vessel temperature of 70 °C. Additionally, the effect of heat conduction becomes less important as $\tau \gg t_L$. Similar curves have been calculated analytically by Svaasand *et al* (1995a), who assumed that instantaneous heating of the red blood cells to 100 °C occurs.
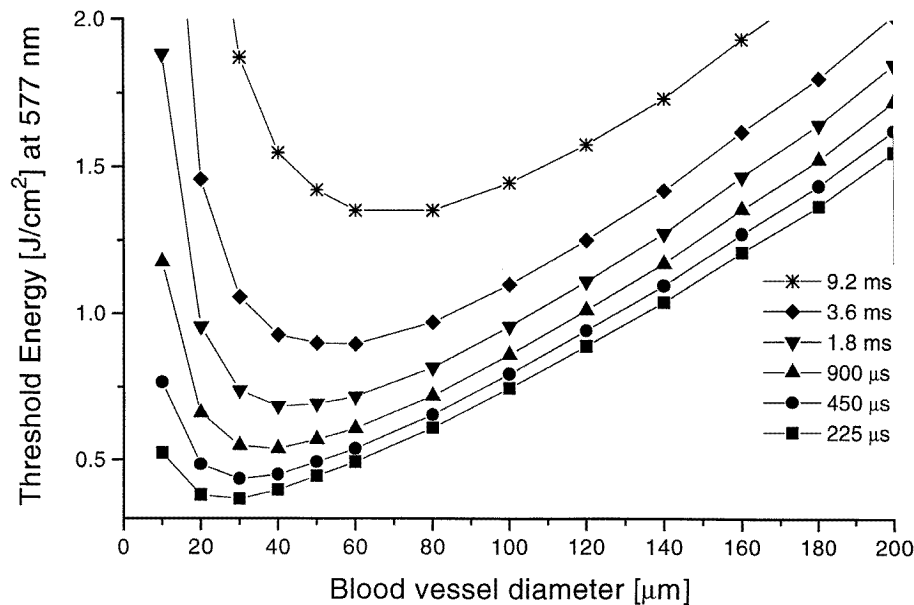
Figure 5. Threshold radiant exposures at 577 nm necessary to raise the average temperature of a single blood vessel, its centre located at 0.25 mm dermal depth, to 70 °C as a function of blood vessel diameter and laser pulse duration from Monte Carlo fluence rate computations and solution of the bio-heat diffusion equation in a 1 mm × 1 mm × 1 mm skin volume with 50 μm epidermal thickness. Epidermal absorption and scattering parameters were 1.8 mm^{-1} and 47 mm^{-1} and $g = 0.79$, respectively; dermal parameters 0.25 mm^{-1} and 13.1 mm^{-1} and $g = 0.79$, respectively; blood parameters 35.4 mm^{-1} and 47 mm^{-1}, and $g = 0.995$, respectively.

The results (figure 5) suggest that laser irradiated ($\lambda = 577$ nm) 30 μm diameter PWS blood vessels (or 40 μm at 585 nm, see de Boer *et al* 1996), require the lowest fluence (0.45 ms pulse) for irreversible injury; therefore, vessels of this diameter are the deepest vascular dermal structures that can be irreversibly injured with such pulse durations. Longer pulse durations (1–10 ms) that have been described as optimal (Anderson and Parrish 1981, Pickering *et al* 1989, van Gemert *et al* 1995a), require a considerably higher fluence and, consequently, the risk of adverse effects (e.g., epidermal damage) is higher. Results similar to figure 5 have recently been used to model laser treatment of PWSs containing multiple vessels of different diameter (de Boer *et al* 1996). The results suggest that selectivity for irreversible thermal injury can be achieved when the laser pulse duration matches the blood vessel diameter at the minimum of figure 5. Alternatively, blood vessels may remain resistant to treatment if these conditions are not met.

4.3. Optimal radiant exposure, laser spot size and repetition rate

The optimal radiant exposure produces the deepest PWS vascular injury while sparing the basal membrane. Epidermal melanin concentration is important, although cooling the skin surface using short (ms) cryogen spurts can protect the basal layer during laser irradiation, allowing use of a higher radiant exposure and deeper vascular injury than would otherwise be possible (Anvari *et al* 1995a, b, Nelson *et al* 1995).

The optimal spot size produces the deepest fluence distribution per unit of radiant exposure: recent Monte Carlo simulations indicate that currently available 5–10 mm diameter spot sizes are sufficiently large to achieve that goal (see e.g. van Gemert *et al* 1995a).

Whether repetition rate requires optimization is incompletely understood. Preliminary work by Dierickx *et al* (1995b) has shown that 16 multiple pulses, given at 0.1 Hz and 5 J cm^{-2}, produced ulcerations in the treated PWS site. Additional continuous cooling at 10 °C produced excellent clearance without ulcerations.

5. Discussion

Increasing evidence suggests that selective photothermolysis of PWS blood vessels requires selection of laser irradiation parameters based on knowledge of the anatomy and physiology of the microvascular system to be treated. Non-invasive optical and thermal sensing techniques need to be developed to produce a three-dimensional tomographic map of the underlying PWS microcirculation on an individual patient basis throughout an extended treatment protocol.

The three non-invasive sensing techniques described obtain complementary anatomical and physiological data. First, IRT shows epidermal melanin absorption, and diameter, location and temperature rise of PWS vessels heated by incident laser light, providing direct insight on treatment safety and depth achieved per pulse. This method requires use of advanced numerical inversion algorithms. Second, ORS can provide average optical PWS characteristics, such as dermal fractional blood volume, average superficial and deep vessel diameter and epidermal melanin absorption. ORS defines PWS colour, and has been used to assess treatment progress. Third, OLCR has the potential to determine the depth and diameter of PWS vessels in their three-dimensional dermal matrix, as well as percentage oxygen saturation and blood flow. Once fully developed, OLCR will allow evaluation of treatment depth following each pulse, and the biological response of the PWS microcirculation in response to laser irradiation. OLCR, albeit the most promising of the diagnostic methods, is an advanced version of an interferometric technique which requires further technical development. Clinical testing of the three methods in well planned trials is required to evaluate their roles in the future treatment strategy of PWS.

If anatomical and physiological data on PWS were available, current models predicting irreversible vascular injury due to light and heat propagation would be insufficiently developed to select the optimal treatment parameters for complete blanching in the fewest possible treatment sessions. Although thermal modelling of PWS laser tissue interaction has probably evolved to an adequate level, the lack of experimentally verified criteria for irreversible vascular injury hampers clinical progress.

In conclusion, PWS treatment faces a new era where non-invasive sensing techniques for precise definition of the vascular anatomy and physiology are being combined with laser parameters selected on an individual patient basis throughout an extended treatment protocol. Development of the sensing techniques as well as criteria for treatment parameters are rapidly progressing, and clinical trials are forthcoming.

Acknowledgments

References

Anderson R R and Parrish J A 1981 Microvasculature can be selectively damaged using dye lasers: a basic theory and experimental evidence in human skin *Lasers Surg. Med.* **1** 263–70
——1983 Selective photothermolysis: precise microsurgery by selective absorption of pulsed radiation *Science* **220** 524–7
Anvari B, Milner T E, Tanenbaum B S, Kimel S, Svaasand L O and Nelson J S 1995a Selective cooling of biological tissues for thermally mediated therapeutic procedures *Phys. Med. Biol.* **40** 241–52
Anvari B, Tanenbaum B S, Milner T E, Kimel S, Svaasand L O and Nelson J S 1995b A theoretical study of the thermal response of skin to cryogen spray cooling and pulsed laser irradiation: implications for the treatment of port wine stain birthmarks *Phys. Med. Biol.* **40** 1451–65
Bonner R F and Nossal R 1990 Principles of laser–Doppler flowmetry *Laser–Doppler Flowmetry* ed A P Shepherd and P A Öberg (Dordrecht: Kluwer) ch 2, pp 17–46
de Boer J F, Lucassen G W, Verkruysse W and van Gemert M J C 1996 Diameter dependence of the thermolysis of port wine stain blood vessels on the laser pulse length *Lasers Med. Sci.* **11** 177–80
Dierickx C C, Casparian J M, Venugopalan V, Farinelli W A and Anderson R R 1995a Thermal relaxation of port-wine stain vessels probed *in vivo*: the need for 1–10 millisecond laser pulse treatment *J. Invest. Dermatol.* **105** 709–14
Dierickx C C, Farinelli W A and Anderson R R 1995b Multiple-pulse photocoagulation of portwine stain blood vessels with a 585 nm pulsed dye laser *Lasers Surg. Med.* **57** 261 (abstract)
Goodman D M, Johansson E and Lawrence T E 1992 On applying the conjugate gradient method to image processing problems *Multivariate Analysis: Future Directions* ed C R Rao (Amsterdam: North-Holland)
Goodman J W 1985 *Statistical Optics* (New York: Wiley)
Hopper G S 1993 Forward looking infrared systems *Passive Electro-optical Systems* ed S B Campana (Ann Arbor, MI–Bellingham, WA: ERIM–SPIE)
Huang D *et al* 1991 Optical coherence tomography *Science* **254** 1178–81
Lucassen G W, Svaasand L O, Verkruysse W and van Gemert M J C 1995 Laser energy threshold for thermal vascular injury in a port wine stain skin model *Lasers Med. Sci.* **10** 231–4
Lucassen G W, Verkruysse W, Keijzer M and van Gemert M J C 1996 Light distributions in a port wine stain model containing multiple cylindrical and curved blood vessels *Lasers Surg. Med.* **18** 345–57
Milner T E, Goodman D M, Tanenbaum B S, Anvari B, Svaasand L O and Nelson J S 1996a Imaging laser heated subsurface chromophores in biological materials: determination of lateral physical dimensions *Phys. Med. Biol.* **41** 31–44
Milner T E, Goodman D M, Tanenbaum B S and Nelson J S 1995 Depth profiling of laser heated chromophores in biological tissues using pulsed photothermal radiometry *J. Opt. Soc. Am.* A **12** 1479–88
Milner T E, Smithies D J, Goodman D M, Lau A and Nelson J S 1996b Depth determination of chromophores in human skin by pulsed photothermal radiometry *Appl. Opt.* **35** 3379–84
Mulliken J B and Young A R 1988 *Vascular Birthmarks–Hemangiomas and Malformations* (Philadelphia, PA: Saunders)
Nelson J S, Milner T E, Anvari B, Tanenbaum B S, Kimel S and Svaasand L O 1995 Dynamic epidermal cooling during pulsed laser treatment of port wine stain—a new methodology with preliminary clinical evaluation *Arch. Dermatol.* **131** 695–700
Norvang L T, Fiskerstrand E J, Bakken B, Grini D, Standahl O, Milner T E, Berns M W, Nelson J S and Svaasand L O 1996 *Proc. Medical Applications of Lasers III, SPIE* vol 2623 (Bellingham, WA: SPIE) pp 1-14
Pickering J W, Butler P H, Ring B J and Walker E P 1989 Computed temperature distributions around ectatic capillaries exposed to yellow (578 nm) laser light *Phys. Med. Biol.* **34** 1247–58

Smithies D J and Butler P H 1995 Modelling the distribution of laser light in port-wine stains with the Monte Carlo method *Phys. Med. Biol.* **40** 701–31

Svaasand L O, Fiskerstrand E J, Kopstad G, Norvang L T, Svaasand E K, Nelson J S and Berns M W 1995a Therapeutic response during pulsed laser treatment of port wine stains; dependence on vessel diameter and depth in dermis *Lasers Med. Sci.* **10** 235–43

Svaasand L O, Norvang L T, Fiskerstrand E J, Stopps E K S, Berns M W and Nelson J S 1995b Tissue parameters determining the visual appearance of normal skin and port-wine stains *Lasers Med. Sci.* **10** 55–65

Tan O T 1992 *Management and Treatment of Benign Cutaneous Vascular Lesions* (Philadelphia, PA: Lea and Febiger)

Tan O T, Morrison P and Kurban A K 1990 585 nm for the treatment of port-wine stains *Plast. Reconstr. Surg.* **86** 1112–17

Tan O T, Murray S and Kurban A K 1989 Action spectrum of vascular specific injury using pulsed irradiation *J. Invest. Dermatol.* **92** 868–71

van Gemert M J C, Smithies D J, Verkruysse W, Milner T E and Nelson J S 1997 Wavelengths for port wine stain laser treatment: influence of vessel radius and skin anatomy *Phys. Med. Biol.* **42** 41–50

van Gemert M J C, Welch A J, Pickering J W and Tan O T 1995a Laser treatment of port wine stains *Optical–thermal Response of Laser Irradiated Tissue* ed A J Welch and M J C van Gemert (New York: Plenum) ch 23, pp 789–829

van Gemert M J C, Welch A J, Pickering J W, Tan O T and Gijsbers G H M 1995b Wavelengths for laser treatment of port wine stains and telangiectasia *Lasers Surg. Med.* **16** 147–55

Verkruysse W, Lucassen G W, de Boer J F, Smithies D J, Nelson J S and van Gemert M J C 1997 Modelling light distribution of homogeneous versus discrete absorbers in laser irradiated turbid media *Phys. Med. Biol.* **42** 51–65

Verkruysse W, Lucassen G W and van Gemert M J C 1996 unpublished